Chapter 11
Polarized Electron Sources

Joe Grames and Matt Poelker

Abstract Highly spin polarized electron beams produced from GaAs photocathodes within DC high voltage photoguns have been critical to many accelerator-based nuclear and particle physics experiments. This chapter describes polarized photoemission from GaAs, the main requirements for constructing a DC high voltage electron source, and techniques to control and measure the polarization of the electron beam.

11.1 Introduction

Many accelerator-based nuclear and particle physics experiments require a spin-polarized electron beam [1]. This describes a beam where the electrons within each accelerated bunch have their spin axes aligned in a preferential direction. Electron spin can be thought of as another "tool" in the physicist's tool bag, one that enables enhanced study of nuclear structure, the dynamics of strong interactions, electroweak nuclear physics including parity-violation, physics beyond the Standard Model and more [2]. Electron beams at accelerator storage rings "self-polarize" via Sokolov-Ternov spin-flip radiation, however at other types of accelerators a direct source of polarized electrons is required.

This manuscript has been authored in part by Jefferson Science Associates, LLC under Contract No. DE-AC0506OR23177 with the U.S. Department of Energy. The United States Government and the publisher, by accepting the work for publication, acknowledges that the United States Government retains a non-exclusive, paid-up, irrevocable, world-wide license to publish or reproduce the published form of this work, or allow others to do so, for United States Government purposes.

J. Grames (✉) · M. Poelker
Electron Gun Group, Thomas Jefferson National Accelerator Facility, Newport News, VA, USA
e-mail: grames@jlab.org; poelker@jlab.org

This is a U.S. government work and not under copyright protection in the U.S.;
foreign copyright protection may apply 2023
F. Méot et al. (eds.), *Polarized Beam Dynamics and Instrumentation in Particle Accelerators*, Particle Acceleration and Detection,
https://doi.org/10.1007/978-3-031-16715-7_11

The first polarized electron source for an accelerator, based on photo-ionization of state selected ^{6}Li atoms, was developed at Yale University in the early 1970s for use at the Stanford Linear Accelerator (SLAC) [3]. Somewhat later, a polarized electron source based on the Fano effect in Rb was developed for the Bonn synchrotron [4]. Other polarized sources were developed or proposed during the 1970s, including an improved version of the Li photo-ionization source [5], a source based on the chemi-ionization of metastable He atoms [6], and sources using the Fano effect in Cs [7]. Despite some technical demonstrations, none of these latter sources were ever developed to the point of being operational at accelerators. Following the 1974 demonstration of polarized photoemission from GaAs [8] at low voltage, a high voltage source was constructed at SLAC [9] to conduct the seminal parity violation experiment E122 [10] that verified predictions by Wienberg and Salam and thereby helped to establish the Standard Model of electro-weak physics. Since then, DC high voltage polarized electron sources based on GaAs photocathodes were developed and operated at a number of laboratories, including Nagoya University [11], the Mainz Microtron [12, 13], the MIT-Bates Laboratory [14], NIKHEF [15], Bonn University [16], and CEBAF/Jefferson Lab [17].

There are four basic requirements for constructing a DC high voltage spin-polarized electron source using GaAs photocathodes: (1) atomically clean GaAs photocathode material, (2) an appropriate high voltage cathode/anode accelerating structure free of field emission, (3) ultrahigh vacuum, and (4) a suitable drive laser. Proper attention paid to these subjects will enable the reader to build a good spin-polarized electron source where "good" describes a source that is capable of delivering highly polarized beam at the desired current, for long periods of time.

11.2 GaAs: A Source of Polarized Electrons

GaAs is a direct-transition III-V semiconductor with zincblende crystal structure [18, 19]. It can absorb laser light across the broad visible spectrum but only illumination with near-IR wavelengths provides polarized photoemission. This can be understood by looking at the energy level diagram of GaAs in Fig. 11.1 with both detailed [18, 19] and simplified representations [20] of the band structure, as described in the figure caption. Electron spin-orbit coupling splits the $P_{1/2}$ and $P_{3/2}$ energy levels of the valence band into two states separated by 0.34 eV, which is large enough to avoid optical pumping from the lower energy $P_{1/2}$ state. Polarized photoemission takes advantage of the quantum mechanical selection rules, noting that for circularly polarized laser light, conservation of angular momentum requires an electron's spin-angular momentum quantum number to change by one unit, $\Delta m_j = \pm 1$. Furthermore, some transitions are more favorable than others as indicated by the transition probabilities in Fig. 11.1. So by using circularly polarized laser light with near-bandgap energy, the conduction band can be preferentially populated with a particular spin state.

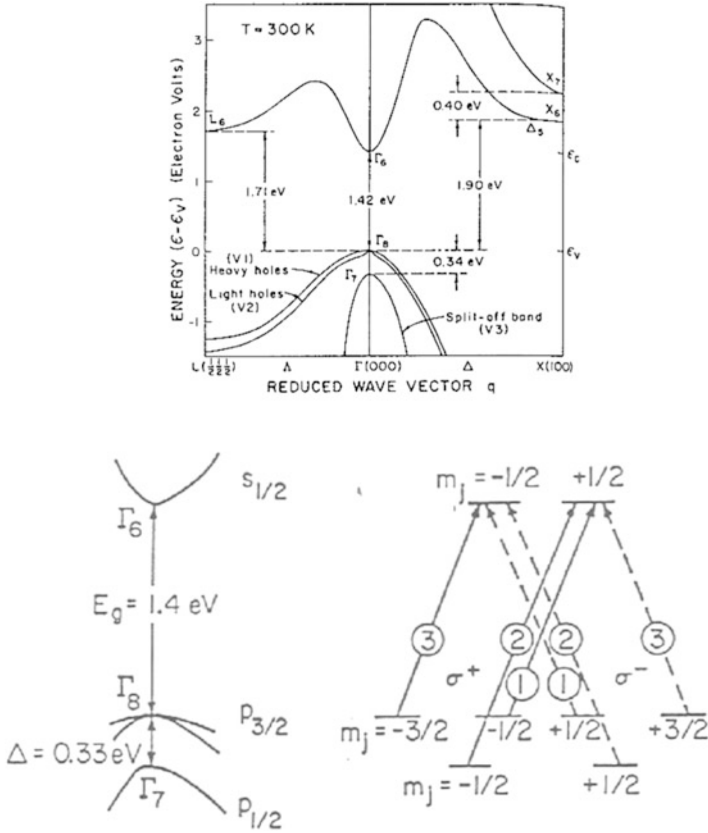

Fig. 11.1 Energy level diagrams of GaAs: (**a**) detailed bandstructure of GaAs [19], (**b**) "close-up" view near valance band maxima/conduction band minima, and (**c**) simplified view showing individual spin-angular momentum states and transition probabilities, circled [20]

Polarization is defined as

$$P = \frac{N^{\uparrow} - N^{\downarrow}}{N^{\uparrow} + N^{\downarrow}}\ , \tag{11.1}$$

where N refers to the number of electrons in the conduction band of each spin state, "up" or "down". For bulk GaAs, the theoretical maximum polarization is 50%, corresponding to three electrons of the desired spin state and one electron with opposite spin. In practice however, maximum polarization from bulk is typically 35%, owing to various proposed depolarization mechanisms such as the Bir-Aronov-Pikus process [21], the D'Yankonov-Perel process [22], the Elliot-Yafet process [23], and radiation trapping [24]. A less academic description simply attributes depolarization to imperfections within the photocathode material that result in reduced diffusion length which serves to prevent electrons from efficiently

reaching the surface of the photocathode, thereby providing more opportunity for the electrons to depolarize on the way out.

The figure of merit of most polarized electron beam experiments scales as P^2I, where I refers to beam current. As such, there is great incentive to increase beam polarization, particularly for experiments that cannot accommodate high current, for example, due to concern over target window failure or target boiling. Significant breakthroughs in polarized electron source development occurred in the 1990s when Nakanishi et al. [25] developed a means to eliminate the heavy-hole/light-hole degeneracy at the valence band maxima by introducing an axial strain within the GaAs crystal. This was accomplished by growing GaAs atop GaAsP which introduces a strain due to the lattice mismatch between the GaAs and GaAsP crystal structures. Polarization as high as ~75% can be obtained from such a structure however photocathode yield, or quantum efficiency QE, is typically very low, just 0.1% (more on QE below). The GaAs surface layer is typically 50 to 100 nm thick. Thicker layers can provide higher QE, but this causes the strain to relax and polarization is reduced.

Today's state-of-the-art high polarization photocathode is the GaAs/GaAsP strained-superlattice structure [26] which consists of a very thin GaAs surface layer (~5 nm) grown atop 10–20 pairs of thin, alternating layers of GaAsP and GaAs. By growing very thin GaAs layers, the strain can be maintained which improves polarization and electrons in sub-surface layers efficiently tunnel through the GaAsP layers. And by using many thin layers of GaAs/GaAsP, the QE can be considerably higher than obtained from a single (thicker) layer of strained GaAs. The net result is polarization ~85% and QE ~1%. Schematic representations of each high polarization photocathode are shown in Fig. 11.2 with plots of polarization versus laser wavelength [27].

Both of the photocathode structures described above were developed [28, 29] thanks to collaborative R&D programs initiated by SLAC via the DOE small business initiative research program. Similar photocathodes have been manufactured by university groups in Japan and Russia [30], with different stoichiometric combinations of Ga, As and P as well as In and Al, that serve to modify the band-gap and correspondingly, the appropriate drive laser wavelength.

The emission of electrons from GaAs is often described as a three-step process [31] involving absorption of light, diffusion of electrons to the surface of the photocathode, and emission of the electrons into the gun vacuum chamber. As described above, absorption of circularly polarized light with near-band gap energy preferentially populates the conduction band with spin polarized electrons. GaAs is a strong absorber with most of the light absorbed within a few hundred nanometers. These electrons diffuse in all directions and those that move toward the surface encounter a potential barrier known as the electron affinity (Fig. 11.3a). A requirement for efficient photoemission is that the GaAs be p-doped [8], which serves to lower the Fermi level throughout the material. The p-doping also serves to lower the conduction band at the surface of the photocathode, which in turn lowers the electron affinity (Fig. 11.3b). Still, no significant photoemission is obtained until the potential barrier is reduced further and this is accomplished by adding a mono-

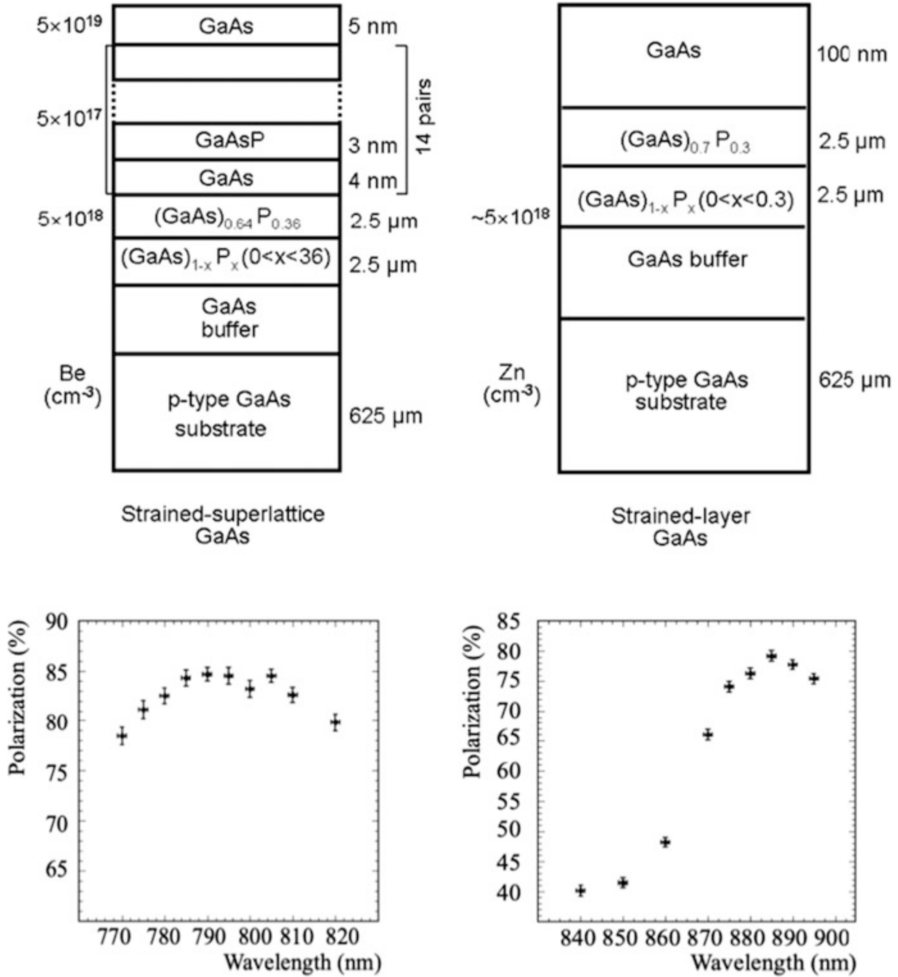

Fig. 11.2 Two types of GaAs photocathode structures that provide high polarization: (left) strained-superlattice GaAs and, (right) strained-layer GaAs

layer of cesium and oxidant (Fig. 11.3c). The process of adding cesium and an oxidant to the photocathode is called “activation”.

All of this sounds relatively simple, however in practice, obtaining the expected amount of photoemission can be difficult because the GaAs surface must be extremely clean and free of contamination on an atomic scale. Unfortunately, there are a number of steps that must be taken to insert a GaAs photocathode into a DC high voltage photogun which means there are many opportunities to contaminate the wafer. And once the photocathode is installed within the photogun, it must remain clean, which means the photogun must function properly while delivering beam. Mostly this means the static vacuum inside the photogun must be extremely low

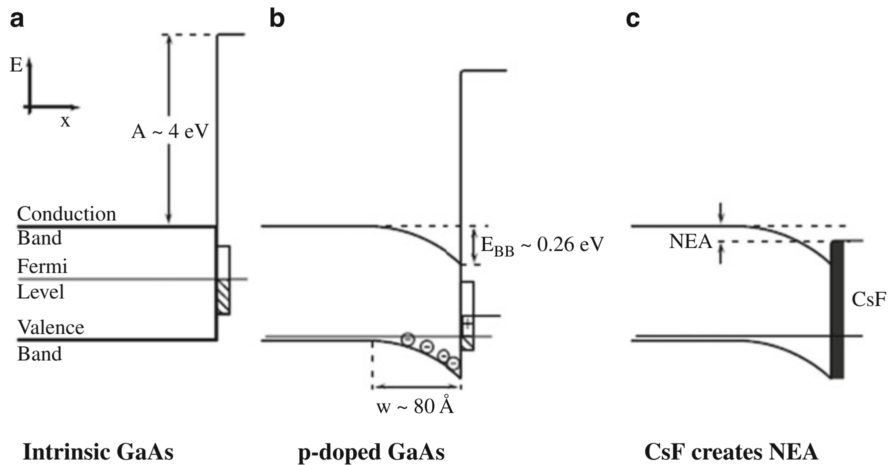

Fig. 11.3 Energy level diagram of GaAs at the vacuum interface. (**a**) Undoped GaAs, (**b**) p-doped GaAs, (**c**) with Cs and oxidant applied to the surface

and must remain low while delivering beam. The sections below describe typical photoguns and the steps required to install clean photocathodes.

11.3 Description of Typical Polarized Photogun

DC high voltage GaAs-based polarized photoguns can be categorized as vent/bake or load-locked. In general, vent/bake guns are considered easier to build but require frequent maintenance whereas load locked photoguns offer more accelerator uptime, at least once reliable sample manipulation has been demonstrated. A brief description of each type is presented below.

11.3.1 Vent/Bake Photoguns

Vent/bake photoguns must be vented to atmospheric pressure each time the photocathode is replaced, and then baked for an extended period of time to recover the necessary vacuum level (more below). A typical vent/bake photogun is shown in Fig. 11.4 and was successfully used at CEBAF/Jefferson Lab for over ten years [17]. All of the features that are needed to activate the photocathode to NEA, bias the photocathode at high voltage, and generate high-quality beam in an ultrahigh vacuum environment are housed in a common vacuum chamber.

The photocathode is attached to the end of a long stalk extending into the gun vacuum chamber through the bore of the large cylindrical insulator. Prior to

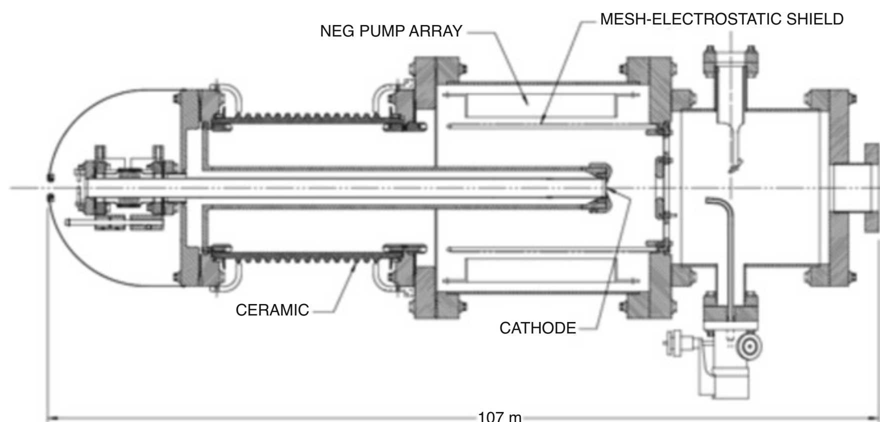

Fig. 11.4 The CEBAF/Jefferson Lab vent/bake -100 kV DC high voltage spin polarized GaAs photogun. It rests in the horizontal plane with the drive laser light introduced through a vacuum window to the right (not shown)

activating the photocathode to NEA, the photocathode must be heated to $\sim$500 °C to liberate loosely bound adsorbed gas. Higher temperatures can "boil off" some of the surface contamination (oxides, in particular) but not carbon. Temperature $>$630 °C must be avoided as this causes the GaAs to decompose due to preferential evaporation of arsenic. To heat the photocathode, the stalk is retracted $\sim$5 cm to avoid heating other parts of the gun and a resistive heater is inserted into the atmospheric side of the stalk in close mechanical contact. When the heat treatment has concluded, the photocathode is allowed to cool to room temperature and then moved back into position within the cathode electrode for activation and beam generation. The cathode electrode has a 25 degree focusing angle and the anode is approximately 6 cm away. This geometry provides optimized transport for CEBAF beam with a maximum field gradient of $\sim$5 MV/m when the cathode electrode is biased at -100 kV. Note that the cathode/anode geometry of each photogun depends heavily on the accelerator's beam specifications (e.g., bunch charge) and is typically determined by performing computer simulations (i.e., field mapping and particle tracking).

Non-evaporable getter (NEG) modules surround the cathode/anode gap providing thousands of liters/sec pumping for hydrogen. A small diode ion pump (not shown) is used to pump inert gases such as helium and methane that are not efficiently pumped by NEGs. The photocathode is activated to NEA using cesium and fluorine (or oxygen) sources located downstream of the anode. During activation, the drive laser can be directed onto the photocathode, or a white light source can illuminate the photocathode from the side using a metallic mirror inside the vacuum chamber. The two chemicals, Cs and NF_3, are applied to the photocathode and metered while monitoring photocurrent, which varies in a "yo-yo" manner with photocurrent begin successively increased and decreased, although

other groups follow different but acceptable protocols. The yo-yo activation process is described below. The chemical application is terminated once photocurrent ceases to increase appreciably, typically after ten yo-yo's, with the net result corresponding to approximately one monolayer of chemical deposition. Cesium originates from a alkali-metal dispenser from SAES Getters and is controlled by applying electrical current through a vacuum feedthrough. The NH_3 is applied using a vacuum leak valve.

As mentioned above, the entire gun structure must be baked each time the photocathode is replaced. Bakeout temperature is typically ∼250 °C and bakeout duration is ∼30 hours, although the bakeout can last longer if there is significant water vapor inside the vacuum chamber, for example due to extensive vacuum chamber modification. High temperature bakeouts necessitate some precautions. For example, bare copper gaskets will oxidize during a bakeout. This is problematic because the oxide layer can "flake off" when flanges are disassembled which sometimes leads to a flange leak during a subsequent bakeout. To prevent this from happening, copper gaskets should be nickel-flashed and silver-plated because these gaskets will not oxidize. Silver-plated bolts are also recommended for the same reason, they do not oxidize. This ensures that nuts and bolts turn freely post-bakeout when gun disassembly is warranted. The NEG pumps can be electrically activated or passively activated to about 60% of their rated pump speed during the bakeout.

Besides the burden of vacuum chamber bakeouts, which take days to complete, the most significant drawback of the vent/bake photogun design is the inadvertent application of cesium on the cathode electrode, which eventually leads to catastrophic field emission, necessitating cathode electrode cleaning or replacement. The design shown in Fig. 11.4 provides about seven full photocathode activations before succumbing to field emission. Other gun designs at other laboratories faired better or worse and in hindsight, results likely depended on the size of the anode hole and location of the cesium dispenser relative to the anode, which define the solid angle of cesium deposition at the photocathode and cathode electrode. Gun designs with small solid angle faired better than those that introduced more cesium on the cathode electrode.

11.3.2 Load/Lock Photoguns

Load-locked photoguns are comprised of multiple vacuum chambers separated by valves, with vacuum improving from one chamber to the next and the best vacuum obtained inside the gun high voltage chamber. Reiterating on comments above, one of the benefits of a load-lock design is that new photocathode samples can be installed without lengthy vacuum bake-outs of the entire gun. Another benefit of the load lock approach is that cesium is not inadvertently applied to the cathode electrode since activation takes place inside another chamber. In this way, the cathode electrode is maintained pristine, and it exhibits no field emission when

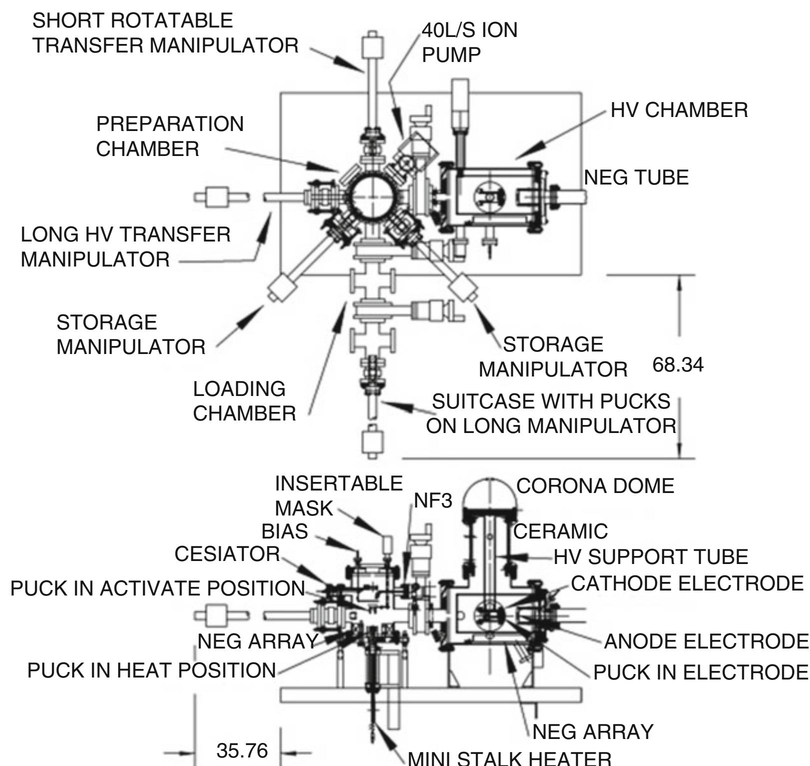

Fig. 11.5 (Top) Plan view shows the complete gun assembly with four vacuum chambers: gun High Voltage Chamber (large bore ceramic insulator design), Preparation Chamber, intermediary chamber and "Suitcase". (Bottom) Side view shows some of the components inside the preparation chamber including a heater that also serves to move the puck toward a mask used to selectively activate only the center portion of the photocathode

biased at high voltage. Historically, most gun groups move to a load lock design for this reason to eliminate field emission.

The CEBAF/Jefferson Lab load lock gun is shown in Fig. 11.5 [32]. It consists of four vacuum chambers: the high voltage chamber, the photocathode preparation chamber, a "suitcase"'chamber used for replacing photocathode samples, and an intermediary chamber that must be evacuated and baked each time the suitcase is attached. The suitcase is normally detached from the photogun and stored elsewhere. This approach helps to reduce the overall footprint of the photogun when in operation. Numerous alternative designs are used at laboratories worldwide [12, 13, 15, 16, 33, 34]. Desirable features incorporated into most designs include the ability to store multiple photocathode samples, to reliably transport a sample from one chamber to the next without dropping, and rapid heating and cooling of samples for fast turn-around at activation.

The high voltage chamber is similar to that of the vent/bake photogun described above, but without the components associated with photocathode activation. NEG pump modules surround the cathode/anode gap and a small ion pump is used to pump inert gas species.

Key features of the preparation chamber include: storage for up to four pucks (each puck supports one photocathode), a mask for selective activation of a portion of the photocathode surface, puck heating to at least 600 °C and good vacuum obtained using NEG and ion pumps. Photocathode activation takes place inside the preparation chamber using cesium and NF_3 similar to those described for the vent/bake photogun. The preparation chamber has four magnetically-coupled sample manipulators: one long manipulator with translation and rotation capability for moving pucks into or out of the gun high voltage chamber cathode electrode, one short manipulator with translation and rotation capability for moving pucks from/onto the heater assembly as well as to transferring pucks to/from the long manipulator, and two short manipulators with translation capability that serve to hold pucks with additional photocathode samples. Care must be taken during the initial commissioning bake of the preparation chamber—the magnetic manipulators can develop excessive friction that limits functionality when heated above $\sim$200 °C. Each magnetic manipulator is attached to a bellows assembly with adjustment screws for proper alignment to the electrode, heater and other manipulators. Pumping inside the prep chamber was provided by 40 L/s ion pump and 1.5 WP-1250 NEG modules from SAES Getters with support rods removed, and coiled into the bottom of the vacuum chamber. Pressure inside the preparation chamber is $\sim 1 \times 10^{-10}$ Torr, which is adequate for making photocathode with high QE, however improved vacuum would provide a longer dark lifetime.

11.4 Operating a DC High Voltage Spin-Polarized GaAs Photogun

Photocathode lifetime of modern DC high voltage GaAs photoguns is limited primarily by ion bombardment [35], the mechanism where residual gas is ionized by the extracted electron beam and transported backward to the photocathode where the ions adversely affect photocathode QE. Consequently, the best GaAs photogun lifetime is obtained by minimizing ion bombardment and this means operating the photogun with exceptionally good vacuum.

11.4.1 Ion Bombardment

Exactly how the ions degrade QE is the subject of much speculation. While it has been determined that ions with sufficient kinetic energy penetrate the surface of the

photocathode [36], it is not known what these ions do to the photocathode. They might damage the GaAs crystal structure or serve as trapped interstitial defects that reduce the electron diffusion length or serve as unwanted dopant species, adversely altering the photocathode energy band structure. Impinging ions might also sputter away the chemicals used to reduce the work function at the surface of the photocathode. Predicting which ions are the most problematic (gas species and energy) awaits a detailed modeling study that considers many parameters including: relevant ion species with appropriate ionization cross sections, accurate trajectories of both ions and electrons, sputtering yield of alkali (cesium) and oxidant (fluorine) used to create the negative electron affinity (NEA) condition at the photocathode surface required for photoemission, and stopping depths of ions within the photocathode. Parameters such as optical absorption length, electron diffusion length and active layer thickness are likely to be important factors, too.

The ions produced by the electron beam are delivered to the photocathode in a manner determined by the electrostatic field of the cathode/anode structure. When the drive laser beam is positioned at the center of the photocathode, all of the ions are delivered to the same location. When the laser beam is moved radially outward, ions are produced at the location of the laser beam and along a "trench" connecting the point of origin to the electrostatic center of the photocathode. Furthermore, ions produced downstream from the anode can be delivered to the photocathode and these ions hit the electrostatic center. A typical "QE scan" of a GaAs photocathode is shown in Fig. 11.6 illustrating QE reduction due to ion bombardment.

The best strategy for minimizing QE decay associated with ion back bombardment is to operate the photogun under excellent vacuum. This includes static vacuum (no beam) and dynamic vacuum (while delivering beam). A small cathode/anode gap is desired, to limit the number of ions created. However, small gaps produce large gradient, and large gradient enhances field emission from the cathode electrode which can significantly degrade gun performance via chemical poisoning of the photocathode surface and enhanced ion bombardment. A comprehensive study [32] showed that the best operating lifetime can be obtained by operating with a laser beam positioned away from the electrostatic center, and with an active area that minimizes the creation of "halo" beam that might not be efficiently transported away from the photogun. Most recently experiments [37] were performed to quantify the improvement in photocathode charge lifetime by biasing the photogun anode with a positive voltage, which repels ions generated downstream of the anode, improving the charge lifetime by almost a factor of two when the anode was biased compared to the usual grounded configuration.

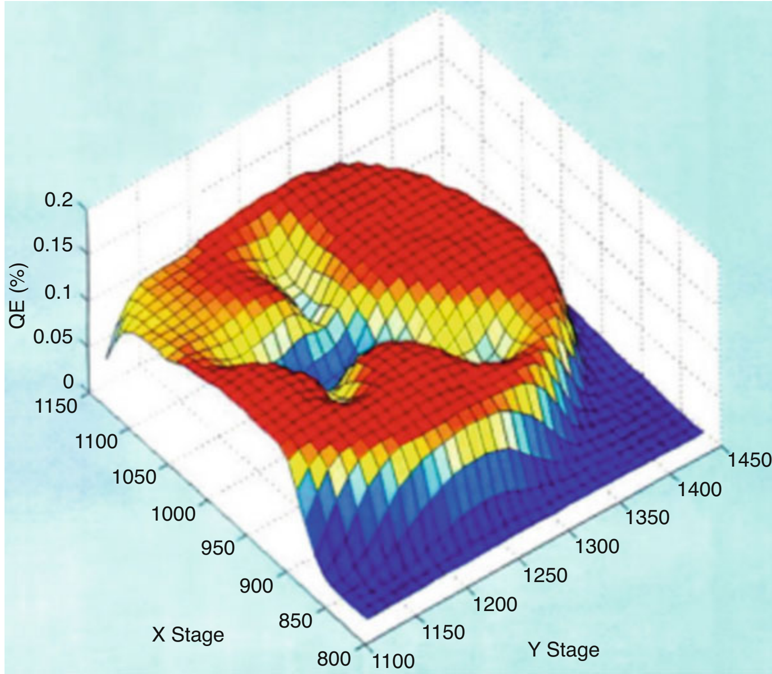

Fig. 11.6 QE measured across the surface of a photocathode that has been damaged by ions. The electron beam was extracted from three different radial locations. Note QE "trenches" that terminate at a common "electrostatic center"

11.4.2 Vacuum

The simple equation below provides remarkably useful insight toward appreciating the vacuum aspects of the photogun:

$$P_{ult} = \frac{GasLoad}{PumpSpeed} \,, \tag{11.2}$$

where P_{ult} is the ultimate pressure inside the gun. Obviously, it is beneficial to make the gas load inside the photogun small and the pump speed large.

To ensure a small gas load inside the photogun, a number of steps must be taken. First, proper UHV techniques must be practiced [38]. This includes constructing the photogun free of contamination. Manufactured parts are typically fabricated without oil or silicone lubricants and all components are cleaned in an ultrasonic bath of alkaline cleaner followed by acetone and hot de-ionized water. It is also very important to ensure that there are no virtual leaks inside the gun (i.e., small spaces with trapped gas). For this reason, internal components are assembled with vented, silver-plated stainless steel screws.

After the photogun has been constructed, it must be evacuated and baked to remove water vapor. Typically, this is accomplished by baking the gun at 250 °C for 30 hours or longer. To assist this process, all CEBAF photoguns are built on tables with an insulating top and large enough to accommodate oven panels that completely surround the gun. For many years heated air was directed into the enclosure using a 4 kW commercial heater system with flowing hot air to assure that the gun structure is heated uniformly without developing significant temperature differentials, however, an occasional failed heater element would lead to cooling and a possible leak due to a thermal shock. Today, very reliable commercial heater bars are routinely used, placed at the bottom of the bakeout oven enclosure, they have sufficient output to raise the oven temperature and if failed they provide for a slow cooling rate of a well insulated enclosure. As mentioned previously, nickel-flashed and silver-plated gaskets are recommended, to avoid oxidation that can lead to flange leaks. Silver-plated high-strength stainless steel bolts and stainless steel nuts can be easily disassembled post-bake. And belleville washers are used on flanges larger than 70 mm to assure reliable sealing during the expansion and contraction cycles of high temperature bakeouts.

When constructed properly, the gas load within the baked photogun originates from hydrogen outgassing from the walls and internal components of the photogun. The typical outgassing rate of 304 stainless steel is 1×10^{-12} Torr-L/sec-cm^2 and with the vacuum pumping from NEGs and ion pump described below, it is not difficult to obtain pressure in the low 10^{-12} Torr range. Hotter bakeouts [38] provide lower outgassing rates and proportionally lower pressure. High current applications benefit from the extra effort to reduce the outgassing rate of photogun components.

Ideally, when the valve to the beamline is opened, the gun vacuum should not degrade appreciably. This means the beamline must be baked and it is a good idea to incorporate a differential pump station near the gun, to isolate gun vacuum from the rest of the accelerator, if space allows it.

As for pumping, all modern DC high voltage spin-polarized GaAs photoguns rely on NEG pumps and a small diode ion pump for inert gases not pumped by NEGs, like He and methane. NEG pumps provide thousands of liters/s pump speed for hydrogen gas, the dominant gas species inside a UHV chamber. NEG pumps are commercial items purchased from SAES Getters and the pumps that rely on ST707 material can be activated at relatively low temperature ($\sim$400 °C). Typically, a photogun design incorporates many NEG modules connected in series and electrically isolated inside the gun. The pumps are activated (i.e., heated) by passing current through them.

11.5 Photocathode Preparation

As mentioned previously, there are a number of steps that must be taken to insert a GaAs photocathode into a DC high voltage photogun, which means there are many opportunities to contaminate the wafer. These steps include:

1. Cut a photocathode sample from a large wafer supplied by the vendor.
2. Anodize the edge of the photocathode to eliminate unwanted photoemission from region not supported by proper electrostatic field. This step can be eliminated if using a mask at activation.
3. Mount the photocathode sample to a support structure that will eventually be positioned within the cathode electrode.
4. Bake the photocathode and support structure to achieve required vacuum level.
5. Heat the photocathode to $>500\,^{\circ}\mathrm{C}$ to liberate loosely bound gas prior to activation to negative electron affinity.

The exact details of these steps vary somewhat depending on the specific photogun design, for example whether a photogun is vented and baked each time the photocathode is replaced, or installed via a load-locked vacuum apparatus where the photocathode is mounted to a small support structure and moved between different vacuum chambers. The text below describes features common to both gun designs and highlights some of the relevant differences.

11.5.1 Cutting GaAs to Shape and Size

GaAs material is typically sold in large circular discs, ~600 μm thick and 50–75 mm diameter, with a flat at one edge to indicate the direction of the cleave plane. This large wafer must be cut into smaller samples for installation into photoguns. Originally, at CEBAF/Jefferson Lab, samples were cut from large wafers using a circular-shaped cutting jig and diamond-paste slurry. The large wafer was sandwiched between glass slides using an acetone-soluble adhesive in an attempt to protect the surface of the photocathode during cutting. This process was time consuming and invariably introduced a significant amount of contamination on the surface of the photocathode, which needed to be removed using strong acids/bases or via hydrogen cleaning. Years ago, this cutting technique was replaced with a far simpler cleaving technique. A diamond-tip scribe is now used to cleave square samples from large wafers. Aside from the diamond-tip scribe, nothing touches the surface of the photocathode material during cleaving and as a result, the photocathode surface is not contaminated.

11.5.2 Anodizing Edge to Limit QE

It is very important to eliminate unwanted and inadvertent photoemission from the edge of the photocathode—photoemission that does not get properly transported away from the gun. Photoemission from the edge of the photocathode follows extreme trajectories, striking the vacuum chamber wall downstream of the gun, and even hitting the anode plate. This degrades vacuum in the gun hastening

photocathode QE decay. One way to eliminate photoemission from the edge, is to anodize edge of the photocathode in an electrolytic bath.

A fixture was devised that holds the photocathode sandwiched between two Viton o-rings. One o-ring prevents electrolytic fluid from contacting the center portion of the front face, and the other o-ring merely provides a surface to securely hold the wafer without breaking it. Clean distilled water with a few drops of phosphoric acid provides adequate pH for anodizing. In just a few seconds, a thick oxide layer is formed on the photocathode edge, that provides no measurable photoemission, and does not evaporate during bakeouts or photocathode heating. For load locked guns, an activation mask can be used to selectively activate only the center portion of the photocathode. This mask eliminates the anodizing step and saves a considerable amount of time.

11.5.3 Mounting a Photocathode

Next, the small photocathode samples are indium soldered to a molybdenum support structure (i.e., the stalk or puck), at $\sim$200 °C, inside a nitrogen-filled glove box. Molybdenum is a good material for supporting the photocathode sample because it has a small coefficient of thermal expansion and is UHV compatible. The indium provides mechanical stability and good heat conduction (the GaAs must be heated to $\sim$500 °C to remove weakly bound gas before activation). A tantalum retaining ring is then placed over the GaAs wafer and crimped in place, to ensure that the GaAs wafer is never inadvertently dislodged from the support structure.

11.5.4 Heating and Activating a Photocathode

The GaAs wafer, mounted to its support structure, is then loaded into the gun vacuum chamber using a nitrogen-filled glove bag. The gun is pumped down using a clean, oil-free rough pump. Once the pressure has dropped sufficiently low as to energize the ion pump on the gun vacuum chamber, the valve to the rough pump is closed. The entire photogun chamber is then baked, as described above. It is important that the GaAs photocathode stay clean during the bakeout. This is accomplished by minimizing the time it takes to vent and pump down the vacuum chamber, and by venting the vacuum chamber with clean, dry nitrogen gas pressurized to assure minimal back diffusion during photocathode exchange. When these precautions are taken, pump down from atmospheric pressure is rapid—the pressure typically falls below 1×10^{-8} Torr within 20 minutes after starting pumping. As further testament to good vacuum practice, the pressure rises no higher than $\sim5\times10^{-8}$ Torr during bakeout.

Once the bakeout is complete, the photocathode can be activated to NEA. This is accomplished by first heating the photocathode to $\sim$500 °C to liberate loosely

Table 11.1 Typical QE and polarization for common GaAs photocathodes

Material	Wavelength	QE	Polarization
"Bulk" GaAs	780 nm	$\sim$10%	$\sim$35%
Strained layer GaAs/GaAsP	850 nm	$\sim$0.1%	$\sim$75%
Strained superlattice GaAs/GaAsP	780 nm	$\sim$1%	$\sim$90%

bound adsorbed gas from the surface of the photocathode. Two hours at temperature is sufficient. Once the photocathode has cooled to $\sim$30 °C, activation begins with successive application of cesium and NF_3 (or oxygen), beginning with cesium. During activation the cathode is biased at ~ -200 V and illuminated with light. On the initial cesium exposure the photoemission current reaches a maximum and then decreases. A typical approach (called the "yo-yo" process) allows the photocurrent to decrease to about half of its maximum value before stopping the cesium exposure. On subsequent exposure to NF_3, the photocurrent rapidly increases to a new maximum, saturates and then slowly decreases. Further exposure to cesium quickly produces a rapid decrease in the photocurrent. Again, the photocurrent falls to about half followed by another nitrogen trifluoride exposure. Typically, ten cycles of Cs-NF_3 are required to reach the final quantum efficiency.

To assess how well the photocathode installation was performed, it is customary to evaluate QE, which is defined as the number of photo-emitted electrons per number of incident photons. It can be written in terms of easily measured quantities:

$$QE = \frac{N_{electrons}}{N_{photons}} = 124\frac{i}{\lambda P}\ , \tag{11.3}$$

where i is photocurrent in μA, λ is laser wavelength in nm, and P is incident laser power in mW. Typical QE values from clean photocathode material illuminated with near-band gap light appropriate for high polarization, are listed in Table 11.1.

11.5.5 Hydrogen Cleaning GaAs

Edge-anodizing is a step that most often introduces contaminants onto the surface of the photocathode. Baking of the photocathode within the gun at high pressure (for example, due to lots of water within the gun) is another opportunity for contamination. There are many recipes for cleaning semiconductor surfaces with wet chemical solutions of strong acids and/or bases, however, experience at Jefferson Lab with wet chemical cleaning techniques was mixed. Moreover, wet chemical cleaning techniques involve significant removal of the surface layer, a situation that is not acceptable when using high polarization photocathodes. So an alternative cleaning procedure using atomic hydrogen was adopted. Atomic hydrogen exposure has been shown to remove surface contaminants such as carbon and oxygen from a wide variety of semiconductors [39–43] . Furthermore, as noted in [44] , hydrogen

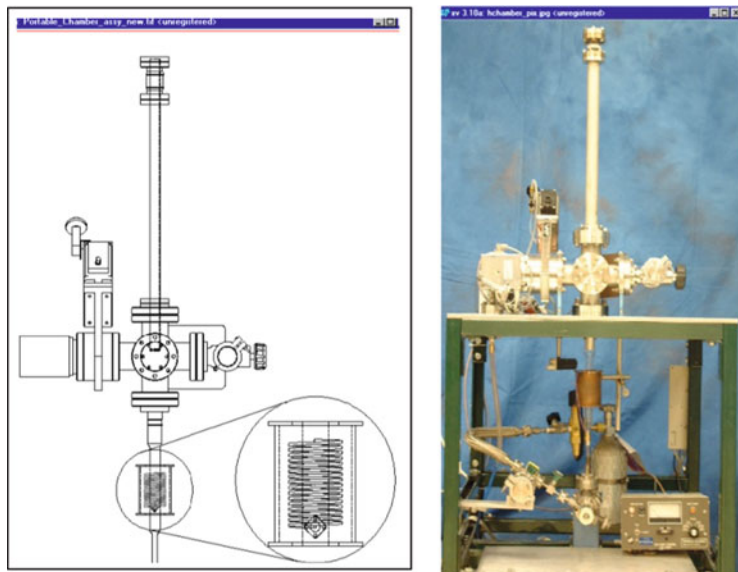

Fig. 11.7 The RF-dissociator, atomic hydrogen cleaning apparatus used at CEBAF/Jefferson Lab

atoms passivate the dangling bonds at the GaAs surface, leaving a relatively inert surface, ideal for gun bakeouts.

RF-dissociators and thermal crackers are common sources of atomic hydrogen. At CEBAF/Jefferson Lab, the RF-dissociator approach is used although there is some concern that this method roughens the photocathode surface. Molecular hydrogen from a small research-grade bottle is fed through a pyrex cylinder at about 20 mTorr (Fig. 11.7). A 12 turn coil surrounds the pyrex tube and a plasma is formed when the applied RF ($\sim$50 W) is resonant with the circuit. Atomic hydrogen exits the chamber through a $\sim$1 mm diameter hole and is guided to the photocathode sample about 15 cm away by an aluminum tube (aluminum has a low recombination rate). The photocathode sample is maintained at 300°C during hydrogen cleaning [41, 42]. A small turbo-molecular pump and an ion pump maintain pressure near the photocathode sample at $\sim 10^{-5}$ mTorr during cleaning, to provide a long mean free path for the atoms and ensure the atoms hit the photocathode before recombining into molecules. Monte Carlo simulations predict that $\sim$2.5% of the total atom flux reaches the photocathode. Under these conditions the atom flux at the cathode is estimated to be $\sim 10^{17}$ atoms/cm^2-sec, assuming 50% dissociation [45].

After hydrogen cleaning, the stalk and photocathode are installed within the photogun using a nitrogen-filled glove bag. Hydrogen cleaning also provides an added benefit, serving to produce a chemically inert surface that helps to keep the photocathode clean during photogun bakeout. Hydrogen cleaning has also been adopted on load locked gun systems, for in situ cleaning.

11.6 Drive Lasers for Polarized Beam

A DC laser light source can be used to make an electron beam at an accelerator but something must be done to create the appropriate RF-time structure necessary for acceleration. Typically this means using RF bunching cavities or RF choppers but bunching introduces energy spread and chopping is very inefficient, with a significant amount of the beam simply thrown away. At CEBAF, these ill-effects were overcome by implementing synchronous photoinjection, a process whereby RF structure is created directly at the photocathode using an RF-pulsed drive laser. In the 1990s, synchronous photoinjection with a GaAs photocathode had not yet been demonstrated. In fact, some thought it would not be possible, suggesting that GaAs would not respond quickly enough to the short-pulse light [46]. However, this concern proved unwarranted and synchronous photoinjection with GaAs is now widely used at many accelerators [47–49].

Modelocked lasers are often used for synchronous photoinjection but gain-switching [50] is the preferred pulse forming technique employed at CEBAF. Gain-switching is a purely-electrical technique that relies on diode lasers. By simply applying $\sim$1 W RF sine wave to the diode laser, $\sim$30 to 50 ps optical pulses can be obtained at repetition rates between 100 to 3000 MHz. This pulse train can be easily locked to the accelerator RF frequency and laser cavity length feedback loops are not required. A gain-switched diode however can only produce a few milliwatts average power and so for most accelerators, a laser amplifier is required to boost power to an acceptable level. At wavelengths between 780 and 850 nm, diode lasers are readily available and single-pass traveling wave tapered stripe diode amplifiers can be used to generate $\sim$100 mW. For higher power applications, fiber-based laser components from the telecom industry are now the best choice. Light at 1560 nm from a fiber-coupled gain switched seed laser can be sent to a fiber amplifier and then frequency doubled to produce Watts of useful light at 780 nm [51] (Fig. 11.8). Similar fiber-based systems are used to generate high power at 532 nm [49].

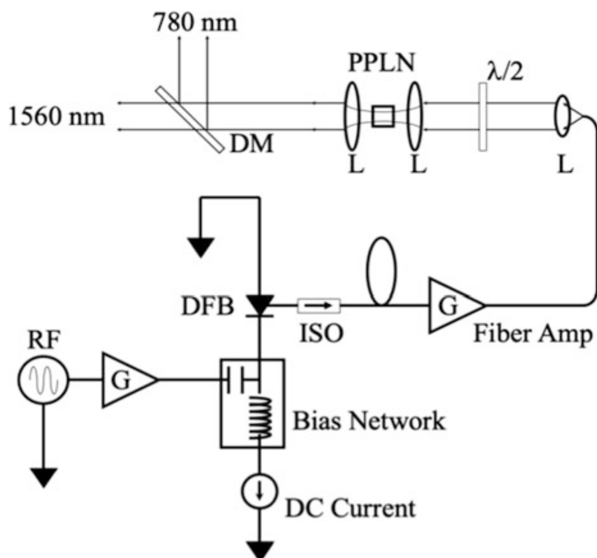

Fig. 11.8 Schematic of the fiber-based laser system with gain-switched diode master oscillator. DFB, distributed feedback Bragg reflector diode laser; ISO, fiber isolator; L, lens; PPLN, periodically poled lithium niobate frequency doubling crystal; DM, dichroic mirror

11.7 Spin Manipulation

Polarized-beam experiments require a specific orientation of the electron spin direction at the target, typically parallel to the direction of beam motion. Moreover, the spin direction must flip sign at some specified frequency. Spin flipping is accomplished by reversing the polarity of voltage applied to an electro-optical element called a Pockels cell, which is located on the drive laser table at the photoinjector. Typically, the polarization direction of the electron beam flips at 30 Hz, and more recently a technique has been developed to flip polarization at a much faster rate up to 1000 Hz [52].

Electrons leave the photocathode with spin direction pointing parallel/antiparallel to the direction of beam motion, depending on the helicity of the laser circular polarization (right or left circular) created by the Pockels cell. But the spin direction precesses in the horizontal plane as the beam passes through the arcs and transport lines to the halls, and this net spin precession must be "cancelled out" by orienting the spin direction at the injector by the opposite amount using a spin manipulator. At CEBAF, a Wien filter is used for spin manipulation [17]. It is a device with static electric and magnetic fields perpendicular to each other and to the velocity of charged particles passing through it, as shown in Fig. 11.9. Unit charged particles with a velocity of $\beta c = E/B$ are undeflected in passing through the Wien filter, while the spin is rotated in the plane of the electric field. A

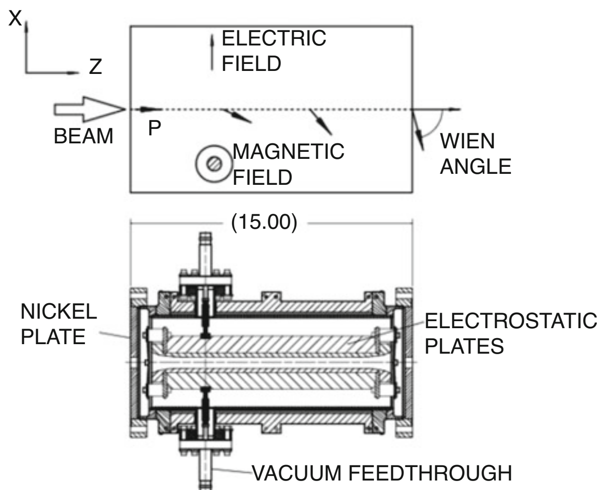

Fig. 11.9 The Wien filter spin manipulator used with CEBAF's second and third polarized electron sources. The magnet is not shown in the cutaway view

window-frame dipole magnet provides the magnetic field. The magnet is terminated at each end with a nickel plate having a 20 mm diameter beam aperture. The full magnet, assembled on the Wien filter vacuum chamber, is carefully mapped with a precision Hall probe. The profile of the electric field plates is calculated, using the code POISSON [53], to produce an electric field profile closely matching the magnetic field profile. The Wien filter is capable of ±110° spin rotation at 100 keV. The calibration and performance of this Wien filter is described in Grames et al. [54].

11.8 Polarimetry

After going through the trouble of making a spin-polarized electron beam, one then needs to measure the magnitude of the polarization. Typically, this is done using Mott polarimetry [55] which can accommodate electron beam energies between a few keV and a few MeV. A Mott polarimeter relies on the scattering asymmetry observed when spin-polarized electrons, with spin vector oriented perpendicular to the scattering plane, scatter from the nuclei of an unpolarized target. To make a polarization measurement, a scattering asymmetry is measured using detectors that count the number of electrons that scatter to the right/left (or up/down) as the direction of the electron spin is flipped by changing the helicity of the photogun drive laser light (via the laser-table electro-optic Pockels cell, described above). The

measured scattering asymmetry is related to beam polarization, P, and the effective Sherman function, S_{eff} as given below:

$$A = \frac{N_r - N_l}{N_r + N_l} = P \times S_{eff} \ . \tag{11.4}$$

The Sherman function, or analyzing power, is a term associated with the physics of the scattering process, and the effective Sherman function describes the same process but modified to account for both single and double elastic scattering into the detector acceptance. The most desirable characteristic of any polarimeter is a large and well-known effective Sherman function however, in practice, this value must be determined by computer simulation and/or detailed experimental measurements, e.g., target thickness extrapolation, or retarding field scans.

The subject of Mott polarimetry is broad enough to be the focus of another book, see e.g. [1, 56]. Suffice to say there are different types of Mott polarimeters that can be loosely categorized according to their electron beam energies: low-voltage retarding field Mott polarimeters, conventional gun-voltage Mott polarimeters and MeV Mott polarimeters. Of these, the MeV Mott polarimeters are the most suited for accelerators; allowing good resolution scintillators and time-of-flight or spectrometer discrimination to isolate the elastically scattered electrons, and lead shielding and veto detectors to suppress the photon background. Plural scattering is significantly reduced and target thickness extrapolation can lead to both precise and accurate($<1\%$) knowledge of the electron beam polarization [57]. For conventional Mott polarimetry at gun voltage ($\sim$100 kV), the effective Sherman function is empirically determined by performing a foil thickness extrapolation to deduce the asymmetry associated with single-scattering events [20]. For retarding field Mott polarimetry [58], a low voltage beam (-200V) is accelerated toward a thick target biased at $\sim$20 kV. Electrons with a broad energy spectrum arrive at the detectors but the single scattering events can be discerned by biasing the detectors at the photocathode voltage.

References

1. J. Kessler, *Polarized Electrons* (Springer, Berlin, 1985)
2. E. Leader, *Spin in Particle Physics* (Cambridge University Press, Cambridge, 2001)
3. M.J. Alguard, J.E. Clendenin, R.D. Ehrlich, V.W. Hughes, J.S. Ladish, M.S. Lubell, K.P. Schuler, G. Baum, W. Raith, R.H. Miller, W. Lysenko, Nucl. Instrum. Meth. **163**, 29 (1979)
4. W. von Drachenfels, U.T. Koch, Th.M. Muller, W. Paul, H.R. Schaeffer, Nucl. Instrum. Meth. **140**, 47 (1977)
5. M.J. Alguard, J.E. Clendenin, P.S. Cooper, R.D. Ehrlich, V.W. Hughes, M.S. Lubell, G. Baum, K.P. Schuler, Phys. Rev. **A16**, 209 (1977)
6. L.A. Hodge, F.B. Dunning, G.K. Walters, Rev. Sci. Instrum. **50**, 1 (1979)
7. P.F. Wainwright, M.J. Alguard, G. Baum, M.S. Lubell, Rev. Sci. Instrum. **49**, 571 (1978)
8. D.T. Pierce, F. Meier, P. Zurcher, Appl. Phys. Lett. **26**, 670 (1975)

9. C.K. Sinclair, E.L. Garwin, R.H. Miller, C.Y. Prescott, *AIP Conference Proceedings*, vol. 35 (American Institute of Physics, Woodbury, NY, 1976), p. 424
10. C.Y. Prescott et al., Phys. Lett. B **77**, 347 (1978)
11. K. Wada, M. Yamamoto, T. Nakanishi, S. Okumi, T. Gotoh, C. Suzuki, F. Furuta, T. Nishitani, M. Miyamoto, M Kuwahara, T. Hirose, R. Mizuno, N. Yamamoto, H. Matsumoto, M. Yoshioka, *Proceedings of the 15th International Symposium on High Energy Spin Physics (SPIN2002), AIP Conf. Proc.*, vol.675 (2003), p. 1063
12. W. Hartmann, D. Conrath, W. Gasteyer, H.J. Gessinger, W. Heil, H. Kessler, L. Koch, E. Reichert, H.G. Andresen, T. Kettner, B. Wagner, J. Ahrens, J. Jethwa, F.P. Schafer, Nucl. Instrum. Meth. A **286**, 1 (1990)
13. K. Aulenbacher, Ch. Nachtigall, H.G. Andresen, J. Bermuth, Th. Dombo, P. Drescher, H. Euteneuer, H. Fischer, D.V. Harrach, P. Hartmann, J. Joffmann, P. Jennewein, K.H. Kaiser, S. Kobis, H.J. Kreidel, J. Langbein, M. Petri, S. Plutzer, E. Reichert, M. Schemies, H.-J. Schope, K.H. Steffens, M. Steigerwald, H. Trautner, Th. Weis, Nucl. Instrum. Methods A **391**, 498 (1997)
14. G.D. Cates, V.W. Hughes, R. Michaels, H.R. Schaefer, T.J. Gay, M.S. Lubell, R. Wilson, G.W. Dodson, K.A. Dow, S.B. Kowalski, K. Isakovich, K.S. Kumar, M.E. Schulze, P.A. Souder, D.H. Kim, Nucl. Instrum. A **278**, 293 (1989)
15. M.J.J. van den Putte, C.W. De Jager, S.G. Konstantinov, V.Ya. Korchagin, F.B. Kroes, E.P. van Leeuwen, B.L. Militsyn, N.H. Papadakis, S.G. Popov, G.V. Serdobintsev, Yu.M. Shatunov, S.V. Shevelev, T.G.B.W. Sluijk, A.S. Terekhov, Yu.F. Tokarev, AIP Conf. Proc. **421**, 260 (1997)
16. W. Hillert et al., *Proceedings of the 14th International Symposium on High Energy Spin Physics (SPIN2000), AIP Conf. Proc.* vol. 570 (2000), p. 961
17. C.K. Sinclair, P.A. Adderley, B.M. Dunham, J.C. Hansknecht, P. Hartmann, M. Poelker, J.S. Price, P.M. Rutt, W.J. Schneider, M. Steigerwald, Phys. Rev. ST Accel. Beams **10**, 023501 (2007)
18. S.M. Sze, *Physics of Semiconductor Devices* (Wiley, New York, 1981)
19. J.S. Blakemore et. al., Semiconducting and other major properties of gallium arsenide. J. Appl. Phys. **53**, R123 (1982)
20. *Investigation of the Physical Properties of Photoemission Polarized Electron Sources for Accelerator Applications*, B. M. Dunham, Ph. D. Thesis, University of Illinois at Urbana-Champaign, 1993
21. G.L. Bir, A.G. Aronov, G.E.Piku, Spin relaxation of electrons due to scattering by holes. Sov. Phys.–ETP **42**, 705 (1976)
22. M.I. D'Yakonov, V.I Perel, Sov. Phys.-JETP **33**, **1053** (1971)
23. R.J. Elliott, Phys. Rev. **96**, 266 (1954); and Y.Yafet, Solid State Phys. **14**, chap. 1 (Academic, San Diego, 1963), p. 1
24. M. Zolotorev, *Effect of Radiation Trapping on Polarization of Photoelectrons from Semiconductors*, vol. 432 (SLAC Pub, Menlo Park, 1994), p. 435
25. T. Nakanishi et.al., Phys. Lett. A **158**(6–7), 345–349 (1991)
26. T. Nakanishi et al., AIP Conf. Proc. **421**, 300–310 (1998)
27. M. Baylac, P. Adderley, J. Brittian, J. Clark, T. Day, J. Grames, J. Hansknecht, M. Poelker, M. Stutzman, A.T. Wu, A.S. Terekhov, Phys. Rev. ST Accel. Beams **8**, 123501 (2005)
28. Strained-layer GaAs photocathode from Bandwidth Semiconductor LLC, Hudson.
29. Strained-superlattice GaAs/GaAsP photocathode, SVT Associates, Inc., Eden Prairie, MN. http://www.svta.com
30. See numerous submissions to the Workshop on Polarized Electron Sources and Polarimeters, published in the *Proceedings of the 18th International Symposium on High Energy Spin Physics (SPIN2008), AIP Conf. Proc.*, vol. 1149 (2009)
31. W.E. Spicer, A. Herrera-Gómez, *Modern Theory and Applications of Photocathodes*, SLAC–PUB 6306 (1993), presented at the 1993 SPIE International Symposium on Imaging and Instrumentation, San Diego
32. J. Grames, R. Suleiman, P.A. Adderley, J. Clark, J. Hansknecht, D. Machie, M. Poelker, M.L. Stutzman, Phys. Rev. ST Accel. Beams **14**, 043501 (2011)

33. M. Breidenbach, M. Foss, J. Hodgson, A. Kulikov, A. Odian, G. Putallaz, H. Rogers, R. Schindler, K. Skarpaas, M. Zolotorev, Nucl. Instrum. Meth. A **350**, 1 (1994)
34. R. Alley, H. Aoyagi, J. Clendenin, J. Frisch, C. Garden, E. Hoyt, R. Kirby, L. Klaisner, A. Kulikov, R. Miller, G. Mulhollan, C. Prescott, P. Sáez, D. Schultz, H. Tang, J. Turner, K. Witte, M. Woods, A. D. Yeremian, M. Zolotorev, Nucl. Instrum. Meth. A **365**, 1 (1995)
35. K. Aulenbacher, *Proceedings of the Workshop on Photocathodes for Polarized Electron Sources for Accelerators, SLAC 432-Rev.* (SLAC, Stanford, CA, 1994), p. 1
36. M.L. Stutzman, J. Grames, in *Proceedings of the 18th International Spin Physics Symposium, AIP Conf. Proc.*, vol. 1149 (2008), p. 1032
37. J.T. Yoskowitz et al., Improving the operational lifetime of the CEBAF photo-gun by anode biasing, in *Proc. IPAC'21*, Campinas, SP, May 2021, pp. 2840–2842. https://doi.org/10.18429/JACoW-IPAC2021-WEPAB104
38. P.A. Redhead, Ultrahigh and extreme high vacuum, in *Foundations of Vacuum Science and Technology*, ed. J.M. Lafferty (Wiley, New York, 1998), p. 625
39. M. Yamada, Y. Ide, Jpn. J. Appl. Phys. **33**, L671 (1994)
40. Y. Ide, M. Yamada, J. Vac. Sci. Technol. A **12**, 1858 (1994)
41. E. Petit et al., J. Vac Sci. Technol. A **10**, 2172 (1992)
42. E. Petit, F. Houzay, J. Vac. Sci. Technol. B **12**, 547 (1994)
43. S. Sugata et al., J. Vac. Sci. Technol B **6**, 1087 (1988)
44. Y. Okada and J. S. Harris, J. Vac. Sci. Technol. B **14**, 1725 (1996)
45. M. Poelker, K.P. Coulter, R.J. Holt, C.E. Jones, R.S. Kowalczyk, L. Young, B. Zeidman, D.K. Toporkov, Phys. Rev. A 50 2450 (1994); and C. Baumgartner et al., Nucl. Intrum. Meth. A **508**, 268 (2003)
46. C.D. Park, S.M. Chung, X. Liu, Y. Li, J. Vac. Sci. Technol. A **26**, 1166 (2008)
47. K. Aulenbacher, H. Euteneuer, D.V. Harrach, P. Hartmann, J. Hoffmann, P. Jennewein, K.H. Kaiser, H.J. Kreidel, H.J. Leberig, C. Nachtigall, E. Reichert, M. Schemies, J. Schuler, M. Steigerwald, C. Zalto, *Proceedings 6th European Particle Accelerator Conference (EPAC98)*, ed. by S. Meyers, L. Lilijeby, C. Petit-Jean-Genaz, J. Poole, K.-G.Rensfeldt (Institute of Physics Publishing, Bristol, Philadelphia, 1998), pp. 1388–1390
48. S. Benson, G. Biallas, C. Bohn, D. Douglas, H.F. Dylla, R. Evans, J. Fugitt, R. Hill, K. Jordan, G. Krafft, R. Legg, R. Li, L. Merminga, G.R. Neil, D. Oepts, P. Piot, J. Preble, M. Shinn, T. Siggins, R. Walker, B. Yunn, Nucl. Instrum. Meth. A **429**, 27 (1999); other JLab FEL-related publications are available at http://www.jlab.org/FEL/felpubs/
49. See Working Group 103 report from ERL09 which includes a description of the Cornell fiber-based drive laser, in *Proceedings of ERL09, 45th ICFA Beam Dynamics Workshop*, June 8–12, 2009 Ithaca, New York
50. M. Poelker, Appl. Phys. Lett. **67**, 2762 (1995)
51. J. Hansknecht, M. Poelker, Phys. Rev. ST-AB **9** 063501 (2006)
52. http://www.jlab.org/accel/inj_group/laser2001/pockels_files/pockels_switch_notebook.htm
53. K. Halbach, Lawrence Livermore National Laboratory Technical Report No. UCRL-17436, 1967
54. J.M. Grames, C.K. Sinclair, J. Mitchell, E. Chudakov, H. Fenker, D.E. Higinbotham, M. Poelker, M. Steigerwald, M. Tiefenback, C. Cavata, S. Escoffier, F. Marie, T. Pussieux, P. Vernin, S. Danagoulian, V. Dharmawardane, R. Fatemi, K. Joo, M. Zeier, V. Gorbenko, R. Nasseripour, B. Raue, R. Sulieman, B. Zihlmann, Phys. Rev. ST-AB **7**, 042802 (2004)
55. T.J. Gay, F.B. Dunning, Rev. Sci. Instrum. **63**(2), 1635 (1992)
56. *Handbook of Accelerator Physics and Engineering*, ed. by A. Chao, K. Mess, M. Tigner, F. Zimmermann, 2nd edn. (World Scientific Publishing Company, Singapore, 2013), pp. 756–758
57. J.M. Grames, C.K. Sinclair, M. Poelker, X. Roca-Maza, M.L. Stutzman, R. Suleiman, Md.A. Mamun, M. McHugh, D. Moser, J. Hansknecht, B. Moffit, T.J. Gay, Phys. Rev. C **102**, 015501
58. J.L. McCarter, M.L. Stutzman, K.W. Trantham, T.G. Anderson, A.M. Cook, T.J. Gay, Nucl. Instrum. Meth. A **30–36** (2010)

Open Access This chapter is licensed under the terms of the Creative Commons Attribution 4.0 International License (http://creativecommons.org/licenses/by/4.0/), which permits use, sharing, adaptation, distribution and reproduction in any medium or format, as long as you give appropriate credit to the original author(s) and the source, provide a link to the Creative Commons license and indicate if changes were made.

The images or other third party material in this chapter are included in the chapter's Creative Commons license, unless indicated otherwise in a credit line to the material. If material is not included in the chapter's Creative Commons license and your intended use is not permitted by statutory regulation or exceeds the permitted use, you will need to obtain permission directly from the copyright holder.